CO_2 methanation over Co–Ni catalysts

Olena V. Ishchenko[1], *Alla G.* Dyachenko[1], *Andrii V.* Yatsymyrskiy[1], *Tetiana M.* Zakharova[1], *Snizhana V.* Gaidai[1], *Vladyslav V.* Lisnyak[1,2], and *Ruslan* Mariychuk[2,*]

[1]Taras Shevchenko National University of Kyiv, Chemical Faculty, 01601 Kyiv, Ukraine
[2]Prešov University in Prešov, Department of Ecology, 080 01 Prešov, Slovakia

Abstract. One of the major goals when creating new energy systems is to provide clean and affordable energy. Currently, there is an excessive increase in the cost of fossil fuels and natural gas because of increased energy consumption and the inability to meet demand. That is why it is necessary to find reliable renewable energy sources and processes that will produce energy materials without toxic by-products in order to preserve the environment and to ensuring sustainable development and a strong economy. From environmental safety reasons, this need has led to the development of the catalytic synthesis of energetic materials from greenhouse gases; in particular, this paper proposes an efficient approach to producing methane by hydrogenation of carbon dioxide over Co–Ni catalysts.

1 Introduction

Atmospheric pollution, the greenhouse effect, and global warming are still the most actual environmental problems of humanity. For example, gaseous carbon dioxide (CO_2) absorbs heat in the Earth's atmosphere and keeps the atmosphere warmer than it otherwise would be. Because of the increase in CO_2 emissions into Earth's atmosphere and oceans, climate change affects peoples and natural systems. Nowadays, there are many technologies preventing atmospheric pollution, including catalytic conversion and adsorptive concentrating of CO_2 at temperatures close to ambient. By the Sabatier methanation of CO_2, one can bind the excess greenhouse CO_2 and convert it, reducing with hydrogen (H_2), into methane (CH_4).

$$CO_2 + 4H_2 \leftrightarrow CH_4 + 2H_2O \quad (1)$$

Such utilization of CO_2 can decrease atmospheric pollution and open up a promising new source of renewable energy [1-3]. Typically, the forward Sabatier reaction takes place at high temperatures and pressures with a catalyst. The literature presents data on catalytic methanation [4-8]. Catalysts based on heavy metals—Ni, Co, Fe, Mn, Cu, and Zn [5, 9-14] and noble metals—Pt, Pd, Rh, and Ru [15, 16] are of special interest. From the reasons of the economy, it is more reasonable to use cheap heavy metal catalysts [17-19]. The

* Corresponding author: ruslan.mariychuk@unipo.sk

selectivity of the methanation depends on the reaction conditions. In fact, carbon monoxide (CO) can be produced via the reverse water-gas shift reaction.

$$CO_2 + H_2 \rightarrow CO + H_2O \quad (2)$$

This reaction can start the Fischer-Tropsch process converting CO into various light hydrocarbons.

$$nCO + (2n+1)H_2 \rightarrow C_nH_{(2n+2)} + nH_2O \quad (3)$$

At the moment, there is no consensus on the mechanism of catalytic hydrogenation of CO_2 [20-22]. A significant part of effective combinations of the active phase, promoter, and catalyst carrier remains unexplored. Consequently, the search for advanced methanation catalysts and the study of the mechanism of this reaction, the problems facing industrial scientists from the end of the 20th century, remain relevant today.

.

2 Experimental

A series of bimetallic $Co_{100-x}Ni_x$ catalysts, where x is the mass percentage of metal, was obtained by wet route reported elsewhere in [23, 24]. To prepare $Co_{100-x}Ni_x$ catalysts, where x = 0, 10, 15, 20, 25, 40, 65, 70, 80, 85, 90, and 100 mass%, the calculated amounts of powdered Co and Ni metals (99.95%, Aldrich) were mixed and dissolved completely in concentrated nitric acid (55 vol.% HNO_3). This solution was refluxed using a sand bath for 30 min. Then the solution of nitrates was cooled freely to 25 °C; after that, an 18% (w/v) ammonia solution was added under vigorous stirring up to neutral pH. Finally, the resulting solution was concentrated at 100 °C for 4 h to obtain a precipitate. The rest of the solution above the precipitate was evaporated in a porcelain dish. The resulting solid was dried at 180 °C. After drying, it was composed of a mixture of oxides, which was reduced in a gas mixture of 50% vol. hydrogen (H_2) in helium (He) under dynamic gas flow conditions. The reduction treatment was carried out for 2 hours at a reduction temperature of 350 °C and near-atmospheric pressure in the flow reactor.

The catalytic activity of the samples (1 g) was investigated in the same reactor that fed with a gas mixture of 2% vol. CO_2 + 55% vol. H_2 in helium (He). We used H_2 from a generator, while CO_2 (99.8%) and He (99.995%) were from gas cylinders supplied by Linde Gas. The total gas flow was 0.1 L/min. The composition of the gas mixture was measured by on-line gas chromatography on a Shimadzu GC-2014 instrument with a thermal conductivity detector, using He as a carrier gas. Separation of CO_2, CO, and CH_4 gases was done with 5A molecular sieves [21]. The CO_2 conversion to methane at 325 °C was taken as the measure of catalytic activity in this series. The surface area of the $Co_{100-x}Ni_x$ catalysts is about 10 $m^2\ g^{-1}$.

After CO_2 methanation, the surface state of $Co_{100-x}Ni_x$ catalysts (stored under inert gas) was studied employing the thermoprogrammed desorption mass spectrometry (TPD MS) method. In TPD MS experiments, we recorded mass spectra and intensity-time TPD profiles for various masses and then constructed selected single ion profiles as a function of temperature. Measurements were carried out on a quadrupole MX 7304A mass-spectrometer, as a detector of particles desorbing from the surface of catalysts. The TPD MS measurements were performed between 30 and 800 °C at a heating rate of 10 °C min^{-1}.

Scanning electron microscopy (SEM) was used for surface imaging and quantitative analysis of catalysts quenched in the reactor under an inert atmosphere. SEM micrographs were collected on an SEM Zeiss EVO 50 instrument. A region from the sample surface up to 1.0 μm depth was probed by an X-ray beam on an INCA 350 X-ray spectrometer

(Oxford Instruments). We measured at least five points (at the maximum penetration depth of 1.5 μm) using an energy-dispersive X-ray (EDX) microanalysis and computed the averaged microanalysis data for them.

3 Results and Discussion

Table 1 presents the catalytic performance measured at the selected temperature.

Table 1. Methane yield ($X(CH_4)$) at 325 °C against Ni content in $Co_{100-x}Ni_x$ catalysts.

Ni, mass%	0	10	15	20	25	40	65	70	75	80	85	90	100
***X*(CH4), vol.%**	54	61	62	65	59	53	40	59	54	48	42	38	4

From the tabulated data follows that the most active catalysts have low Ni content. The $Co_{80}Ni_{20}$ catalyst has the highest activity, and $X(CH_4)$ is about 65%. Increasing the Ni content in the $Co_{100-x}Ni_x$ catalysts reduces the value of $X(CH_4)$. For the least active $Co_{35}Ni_{65}$ catalyst, $X(CH_4)$% is about 40%. For high active and low active catalysts, CO_2, CO, and CH_4 contents *vs*. temperature are given in Fig. 1. At heating, the high active $Co_{80}Ni_{20}$ catalyst (Fig. 1a) shows a rapid increase in $X(CH_4)$.

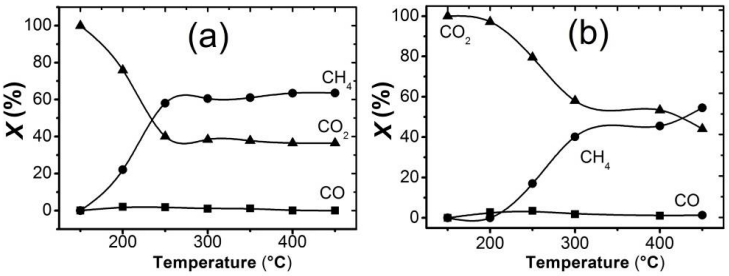

Fig. 1. Contents of CO_2, CO, and CH_4 in the reaction mixture against the reactor temperature in the presence of (a) $Co_{80}Ni_{20}$ and (b) $Co_{35}Ni_{65}$ catalysts.

Beginning from 250 °C, the values of $X(CH_4)$ reach the 60% saturation point. The composition of the reaction mixture in the presence of the $Co_{35}Ni_{65}$ catalyst (Fig. 1b) shows a gradual increase of $X(CH_4)$ with increasing temperature. In the presence of this catalyst, $X(CH_4)$ reaches a value of 54% at 450 °C. This temperature is 200 °C higher than that for the $Co_{80}Ni_{20}$ catalyst. For both catalysts, we found the formation of small amounts of CO (up to 3%). The latter is an undesirable reaction by-product.

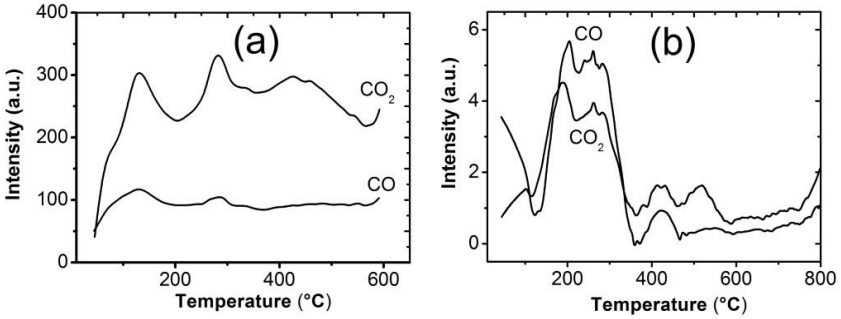

Fig. 2. CO (m/z 28) and CO_2 (m/z 44) TPD profiles for (a) $Co_{80}Ni_{20}$ and (b) $Co_{35}Ni_{65}$ catalysts.

In Fig. 2, we compared the TPD MS profiles for $Co_{80}Ni_{20}$ and $Co_{35}Ni_{65}$ catalysts; they exhibited the highest and the lower activity in CO_2 methanation, correspondingly. For the $Co_{80}Ni_{20}$ catalyst, Fig. 2a shows CO_2 and CO desorption peaks at 134, 280 and 430 °C. According to TPD MS data, the intensity of the CO_2 profile is three times more than that of CO.

For the $Co_{35}Ni_{65}$ catalyst, both CO_2 and CO desorption peaks are registered at 200, 270, 430, and 510 °C (Fig. 2b). Here we observed the reverse situation when the intensity of the CO profile exceeds a little that of the CO_2 profile. This observation correlates with the low activity of the $Co_{35}Ni_{65}$ catalyst. Because of strong bonding with the metal surface on the catalyst's active sites, and due to the fact that CO interacts slowly with hydrogen, chemisorbed CO molecules block the surface sites of the low-active catalyst, as reported earlier in [22]. Consequently, the strong chemisorption inhibits the CO conversion to intermediates of the formate series and methane. The same situation was observed earlier for the CO-PROX and CO oxidation reactions [24-26].

A small amount of CO adsorbed on the active $Co_{80}Ni_{20}$ catalyst suggests that the hydrogenation process of CO passes through the formate residues, and it is the fast process. Confirmation of this assumption is the TPD profiles of the catalytic reaction intermediates and the product of the complete conversion; they are adsorbed on the $Co_{80}Ni_{20}$ catalyst (Figs. 3a and 3b).

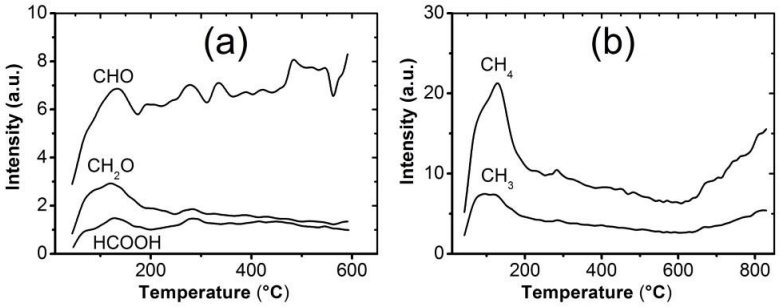

Fig. 3. TPD profiles for the $Co_{80}Ni_{20}$ catalyst. (a) CHO (m/z 29), CH_2O (m/z 30), and HCOOH (m/z 46) and (b) CH_3 (m/z 15) and CH_4 (m/z 16).

CHO*, CH_2O*, and HCOOH* are intermediates of the process of gradually replacing the oxygen atoms of CO_2 with hydrogen atoms on the active catalyst sites. It should be noted that we observed desorption peaks of all the intermediate particles at 130 °C only for the active catalyst (Fig. 3a). The product of the total conversion desorbs from the surface of the active catalyst, and the profile of CH_4 (m/z 16) showed peaks at 80 and 130 °C (Fig. 3b). The desorption profile of CH_3* (m/z 15) coincided well with that of CH_4. This confirms that m/z 16 is from CH_4, and it cannot be assigned to O* of OH from water dissociated under electron impact ionization.

Based on assumptions about the mechanism of the reaction, considering the TPD data, CO_2 molecules can adsorb on the surface of $Co_{100-x}Ni_x$ catalysts during the course of CO_2 hydrogenation. This process can take place on different active catalyst sites having diverse activation energy. After adsorption, the CO_2 molecule dissociates on CO and O. By desorption peak temperatures, the following forms of CO can be distinguished: physisorbed α_1-form (up to 100 °C), weakly chemosorbed α_2-form (100–200 °C), strongly chemosorbed α_3-form (200–300 °C), and α_4-form (above 300 °C).

By comparing TPD profiles for the active and non-active catalysts (Figs. 2 and 3), we assume that both α_2- and α_3-forms of CO impact on the catalytic methanation. For the catalyst showed the highest activity, we observed intensive desorption of CH_4, CHO*, CH_2O*, COO*, and CO (in the α_2-form) at the same temperature of 130 °C. If the

desorption of the aforementioned particles is observed at different peak temperatures, the activity of such a catalyst is reduced.

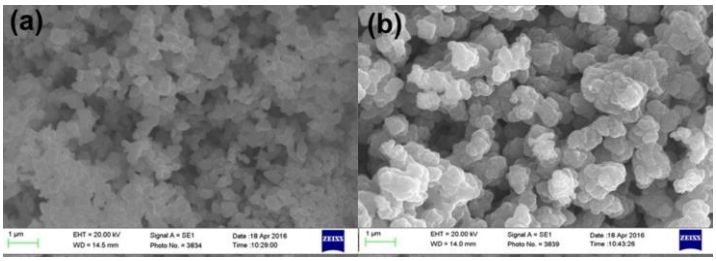

Fig. 4. SEM micrographs of (a) Ni_{100} and (b) Co_{100} catalysts.

SEM micrographs of Ni_{100} and Co_{100} catalysts after the reaction showed that both metal catalysts are highly dispersed with a wide particle size distribution (Fig. 4). The Ni_{100} catalyst is composed of rounded 0.1-0.5 μm agglomerated granules (Fig. 4a). Likely, these granules comprise smaller particles. Figure 4b showed that it is difficult to isolate individual particles for the Co_{100} catalyst forming by large aggregates in the size of several micrometers, which have a layered, scaly structure. One can assume that the Co aggregates grow by laying new portions of the metal into formed particles. In contrast, the growth of Ni aggregates takes place by binding the already formed 0.1-0.5 micron Ni particles. Results of quantitative microanalysis showed the Ni_{100} catalyst contains 99.4 mass% Ni, and 0.6 mass% O. Contrasting the Ni_{100} catalyst, we registered intensive surface oxidation for the Co_{100} catalyst containing 83.9 mass% of Co, and 16.1 mass% of O.

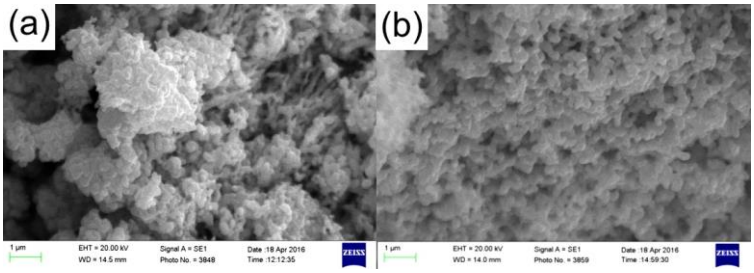

Fig. 5. SEM micrographs of (a) $Co_{80}Ni_{20}$ and (b) $Co_{35}Ni_{65}$ catalysts.

The $Co_{80}Ni_{20}$ catalyst has a layered, scaly microstructure structure (Fig. 5a). This microstructure more resembles that of the Co_{100} catalyst than that of the Ni_{100} catalyst. Besides, the SEM imaging of the particles in the $Co_{80}Ni_{20}$ catalyst revealed linear filamentous formations of up to 0.2 microns in diameter (Fig. 5a). The SEM-EDX analysis showed that the catalyst contains 18.9 mass% Ni, 68.0 mass% Co, and 13.1 mass% O. Just as the Co_{100} catalyst, this catalyst is more oxidized than the $Co_{35}Ni_{65}$ catalyst. The $Co_{35}Ni_{65}$ catalyst contains lesser Co and has a microstructure similar to that of the Ni_{100} catalyst (cf. Fig. 4a and Fig. 5b). In the SEM micrograph (Fig. 5b), one can see small agglomerated granules constituting the $Co_{35}Ni_{65}$ catalyst. From the SEM-EDX analysis, this catalyst contained 69.4 mass% of Ni, 30.1 mass% of Co, and 0.5 mass% of O. The surface of this metal catalyst is seen to have nearly no oxidized metal components. As follows, the catalytic efficiency of bulk $Co_{100-x}Ni_x$ catalysts depends on the level of surface oxidation. To prepare a selective and effective catalyst for the forward Sabatier reaction, one should take into consideration the content of Co in the $Co_{100-x}Ni_x$ catalysts. Because the Co_{100} catalyst showed a higher ability to be oxidized than the Ni_{100} catalyst, the Co component in the $Co_{100-x}Ni_x$ catalysts might be responsible for the surface oxidation.

4 Conclusions

Here we reported the results of CO_2 methanation over the $Co_{100-x}Ni_x$ catalysts prepared by reduction with hydrogen. The bimetallic $Co_{100-x}Ni_x$ catalysts with a low Ni concentration showed higher catalytic activity towards the hydrogenation of CO_2. TPD MS experiments proved that the surface covered by both α_2- and α_3-forms of adsorbed CO molecules is of direct relevance to passaging the catalytic methanation with formate as a reaction intermediate. The SEM-EDX analysis demonstrated the highest surface oxidation for the most active $Co_{80}Ni_{20}$ catalyst (up to 13 at% O) as compared to the $Co_{35}Ni_{65}$ catalyst (up to 1 at% O).

The authors thank the Ministry of Education and Science of Ukraine for the financial support under the State budget program [0119U100167].

References

1. M. Mikkelsen, M. Jorgensen, F.C. Krebs, Energy Environ. Sci. **3**, 43 (2010)
2. S. Ronsch, J. Schneider, S. Matthischke, et al., Fuel. **166**, 276 (2016)
3. X. Su, J.H. Xu, B.L. Liang, et al., J. Energy Chem., **25**, 553 (2016)
4. S. Chaemchuen, N.A. Kabir, K. Zhou, et al., Chem. Soc. Rev. **43**, 9304 (2013)
5. B. Miao, S.S.K. Ma, X. Wang, et al., Catal. Sci. Technol. **6**, 4048 (2016)
6. J. Gao, Q. Liu, F. Gu, et al., RSC Adv. **5**, 22759 (2015)
7. A. Westermann, B. Azambre, M.C. Bacariza, et al., Appl. Catal., B. **59**, 314 (2015)
8. P. Frontera, A. Macario, M. Ferrano, et al., Catalysts. **7**, 59 (2017)
9. K. Stangeland, D.Y. Kalai, H. Li, et al. Appl. Energy, **227**, 206 (2018)
10. J. Aschok, M.L. Ang, S. Kawi, Catal. Today, **281**, 304 (2017)
11. H. Lu, X. Yang, G. Gao, et al., Fuel. **183**, 335 (2016)
12. J. Ren, X. Qiu, JZ. Yang, et al, Fuel Proc. Technol., **137**, 204 (2015)
13. V. Yatsimirsky, V. Budarin, V. Diyuk, et al., Adsorp. Sci. Technol. **18**, 609 (2000)
14. V. Budarin, V. Diyuk, L. Matzui, et al., J. Thermal Anal. Calorim. **62**, 345 (2000)
15. Y.G. Chen, K. Tomishige, K. Yokoyama, et al., Appl. Catal. A: Gen. **165**, 335 (1997)
16. D.C. Upham, A.R. Derk, S. Sharma, et al., Catal. Sci. Technol., **3**, 1783 (2015)
17. T. Bligaard, J.K. Nørskov, S. Dahl, et al., J. Catal., **224**, 206 (2004)
18. M.P. Andersson, T. Bligaard, A.L. Kustov, et al., J. Catal., **239**, 501 (2006)
19. J.J. Gamman, G.J. Millar, G. Rose et al., J. Chem. Soc., Faraday Trans., **94**, 701 (1998)
20. W. Wang, S. Wang, X. Ma et al., Chem. Soc. Rev., **40**, 3369 (2011)
21. R. Meshkini Far, O.V. Ischenko, A.G. Dyachenko, et al., Funct. Mater. Lett., **11**, 1850057 (2018)
22. A.G. Dyachenko, O.V. Ischenko, S.V. Gaidai, et al., Fr.-Ukr. J. Chem., **7**, 74, (2019)
23. E.V. Ischenko, L.Y. Matzui, S.V. Gayday, et al., Materials **3**, 572 (2010)
24. V.L. Veselovskyi, O.V. Ischenko, S.V. Gaidai, et al., Catal. Commun. **18**, 137 (2012)
25. V.V. Lesnyak, V.K. Yatsimirskii, I.N. Gut, et al., Russ. J. Phys. Chem. A, **82**, 1456 (2008)
26. V.V. Lesnyak, E.V. Ishchenko, I.N. Gut, et al., Russ. J. Phys. Chem. A, **81**, 874 (2007)